An Experimental Investigation on the Effect of Laser Energy Deposition in an Over-expanded Jet

S Syam[1,*], Gauresh Raj Jassal[1], Bryan E. Schmidt[1]

1: Dept. of Mechanical and Aerospace Engineering, Case Western Reserve University, 2123 Martin Luther King Jr. Drive, Cleveland, OH, 44106

*Corresponding author: syam.s@case.edu, bryan.e.schmidt@case.edu

Keywords: Axisymmetric Over-expanded Jet, Shock Train Structure, Energy Deposition, Perturbation, Self-Aligning Focusing Schlieren.

ABSTRACT

The shock train structure of a supersonic over-expanded jet is the product of the interaction between the jet flow at the nozzle exit and the ambient environment. Although the effect of flow disturbances on the performance of the supersonic inlets has been studied in detail, a limited understanding of the shock train dynamics subject to flow disturbances is available for over-expanded jets. This experimental investigation focuses on understanding the influence of perturbations due to short-duration energy deposition on the shock train structure and its dynamics in an axisymmetric over-expanded Mach 2.52 jet. The flow is perturbed by laser-induced breakdown, creating a shock wave and a high-temperature plasma zone in the shock train. A high-speed self-aligning focusing schlieren system is used to visualize the flow structure variations by measuring the shock angles and Mach disk height and width to characterize the shock train dynamics and the flow structure recovery process. The response of jet flow to the perturbation at the nozzle exit and the pre-reflection point is found to be similar, however, the response of the supersonic jet to the post-reflection energy deposition is significantly different. The damping ratio for the pre-reflection point and nozzle exit cases found are nearly constant for all scenarios whereas it is linearly dependent on the jet chamber pressure for the post-reflection cases. The frequency of the oscillations is found to be the same for all cases and irrespective of the chamber pressure, laser energy, and deposition location, approximately 10 kHz. The transition from Mach to regular reflection and vice versa are observed at a chamber pressure of P_C = 689 kPa. Any perturbation to the shock structure of a supersonic over-expanding jet at close to the steady-state bifurcation condition between Mach and regular reflection will exhibit Mach-to-regular transition or vice versa.

1. Introduction

An over-expanded jet issuing from a converging-diverging nozzle is a canonical compressible flow produced when the nozzle exit pressure falls below the ambient pressure (Anderson, 1990). The pressure difference generates oblique shock waves at the nozzle exit, which interact and reflect

downstream (Hornung, 1986). These continued interactions of the shock waves and expansions at the exit of the supersonic nozzle form a shock train structure in the jet. The first oblique shock waves will either interact via a Mach reflection or a regular reflection, depending on the ratio of the exit and ambient pressures. The Mach reflection tends to occur at lower exit pressures and regular reflection at higher pressures.

Both Mach and regular reflections can also be observed in flows involving supersonic inlets, and the effect of these shock structures on inlet performance is still an active area of research (Hornung, 1986; Takayama & Ben-Dor, 1993; Ben-Dor, 2013). In particular, the transition of the flow from regular reflection to Mach reflection or vice versa as the geometry and/or pressure is varied is of great interest. In general, most transition studies on Mach-regular reflections are carried out in supersonic inlets for flow control and drag reduction applications, and these investigations are performed by varying the wedge angles of the supersonic inlets. Moreover, these supersonic inlet studies report the presence of hysteresis in the transition between Mach and regular reflections, and this phenomenon was investigated in detail by several researchers, both numerically and experimentally (Ben-Dor et al., 2002; Ivanov et al., 2004; Mouton & Hornung, 2008; Ben-Dor, 2013). Recently, researchers have used other techniques, like laser energy deposition, to perturb the flow at the supersonic inlet to investigate this hysteresis (Knight et al., 2003; Yan et al., 2002, 2003; Yang, 2012). The energy deposition by a laser-induced spark creates a shock wave and a hot plasma zone in the flow which locally perturbs the flow and can cause reflection transition due to the local pressure rise and Mach number variation, depending on the laser energy, location, and flow conditions. In a laser energy deposition process, Phuoc & White (2002) report that 22-34% of the total deposited energy is lost as radiation energy, and afterward 51-70% of the energy is consumed by the shock wave, while only 7-8% of the total energy remains in the deposited location as heat. Laser energy deposition is actively being explored in many other applications in fluid dynamics such as combustion (Phuoc, 2006; Singh et al., 2017), drag reduction (Joarder et al., 2017; Joarder, 2019), and flow control (Yan et al., 2003; Yang, 2012).

Although Mach-regular reflection and transition have been studied in detail for supersonic inlets, very few works have been published on these phenomena in over-expanded jet flows (Hadjadj et al., 2004; Shimshi et al., 2009; Matsuo et al., 2011; Zmijanović et al., 2012; Wang & Yu, 2015; Paramanantham et al., 2022). In general, the studies on over-expanded jets are either numerical (Hadjadj et al., 2004; Shimshi et al., 2009; Zmijanović et al., 2012; Wang & Yu, 2015) or theoretical (Wang & Yu, 2015; Paramanantham et al., 2022), and focused on the transition of Mach and regular reflection to understand the flow separation in the planar (2D) or axisymmetric (3D) nozzle jets. Matsuo et al. (2011) reported hysteresis in shock wave reflections in over-expanded jets experimentally by varying the chamber pressure, but it is one of the only ones to do so in the open literature. Hence, there is a gap in the literature on the response of an over-expanded jet shock train to a perturbation.

The main focus of the present study is to investigate the effect of laser energy and deposition

location on the shock train dynamics and the recovery process, as a function of the pressure in the stagnation chamber of the jet, P_C. Unlike in supersonic inlets where the geometry of the inlet determines the shock angle and hence the pressure ratio, the shocks in jets are produced by the pressure difference between the nozzle exit pressure and the ambient pressure, and the resulting shock angle is the one that creates the necessary post-shock pressure. Hence, in this study, the effect of the perturbations on the flow may be markedly different than what is observed in inlet flows. It is also noted that the size of the plasma spark is comparable to the diameter of the jet in the present study, so the strength of the perturbation is expected to be stronger than in inlet studies where the spark size is typically much smaller than the dimensions of the inlet.

2. Experiment

A top-view schematic of the experimental setup and optical diagnostic arrangement is shown in Fig. 1. An axisymmetric converging-diverging nozzle with a design Mach number of 2.52 and an exit diameter of $D = 12.7$ mm is used to create the over-expanded jet. Nitrogen is supplied at a constant pressure p_0 into the plenum which feeds the nozzle. A Continuum Surelite III ND:YAG laser is used in combination with a plano-convex lens of diameter 50.8 mm and focal length 125 mm to create a spark, and deposit energy at the desired location on the shock train. A self-aligning focusing Schlieren (SAFS) system developed by Bathel & Weisberger (2022) is used to visualize the compressible flow structures in the flow at the plane bisecting the nozzle. A Photron NOVA S12 high-speed CMOS camera is used for the experiments. Images were acquired with a pixel size of 0.11 mm/pixel at a resolution of 512×336 pixels and a frame rate of 64 kHz, resulting in a field of view of approximately $4.5D \times 3D$. A 105 mm Sigma macro lens was used as the field lens in the SAFS system, and a 75 mm Nikkor lens was attached to the camera for imaging. A flicker-free 75 W NILA VARSA LED lamp was used as a light source. The Ronchi ruling in the system has a grid size of 10 lines per mm, which allows the fine structures in the shock train to be resolved.

Table 1. Experimental conditions in the present work. Every combination of laser energy level, chamber pressure, and deposition location listed in the table was investigated.

Laser Energy Level (mJ)		
272	578	716
Chamber Pressure P_C (kPa)		
552	689	896
Deposition Location		
Nozzle exit	Pre-reflection	Post-reflection

In this work, twenty-seven different experimental conditions were considered, which are detailed in Table 1. Three different chamber pressures were used for the investigation, where the lowest chamber pressure, i.e. 552 kPa, produced a Mach reflection, and the shock structure transitioned to regular reflection with the increase of chamber pressure at $P_C = 896$ kPa. Three different laser

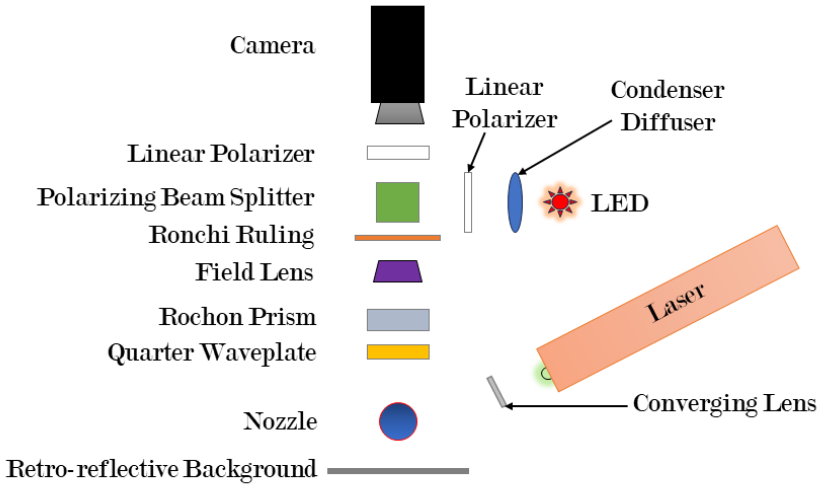

Figure 1. Experimental setup and arrangement of the optical elements

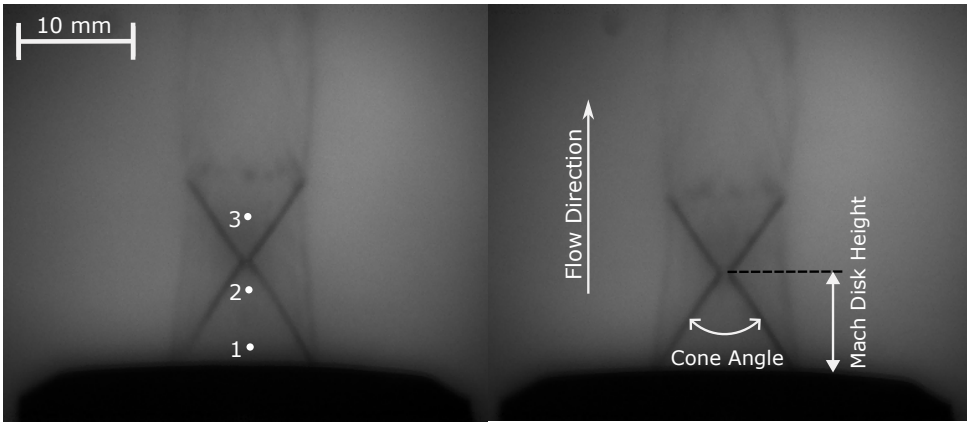

Figure 2. Laser energy deposition locations. 1. Exit of the nozzle, 2. Pre-reflection point 3. Post-reflection point

energy levels were used to examine the effect of perturbation on the shock recovery process and the shock train structure dynamics. The energy was deposited at three different locations in the shock train: the nozzle exit, pre-reflection point, and post-reflection point. The locations are indicated in Fig. 2. Location 1 is selected to examine the effect of energy deposition at the nozzle exit on the shock reflection and Mach disk whereas the intention of location 2 is to study the influence of perturbation on flow when the energy is deposited just before the shock reflection. Finally, location 3 is chosen to investigate to what extent the perturbation signals travel upstream of the flow when the energy is deposited after the Mach disk. Each experiment was performed ten times at each condition to assess repeatability, and to minimize errors that may arise in data processing. The in-house code uses cross-correlation to identify the shock structure at the exit of the nozzle and then applies edge detection to the background-subtracted and de-noised images. Finally, the Hough transform is applied to edge images to recover lines tracing the shock waves, from which the cone angle is obtained geometrically. The images acquired from the experiments were ana-

lyzed automatically to determine the shock angles, Mach disk height, and width variation, with a particular focus on the first shock reflection after the exit of the nozzle.

3. Results

The results obtained from the energy deposition on the shock train at different deposition locations (Fig. 2), at different pressures, and laser energies (Table 1) are presented in this section. The first parameter of interest is the height of the Mach disk above the nozzle exit plane. Second, the transition from Mach to regular reflection is examined.

3.1. Mach Disk Height

The Mach disk height variation due to the laser energy deposition is used to characterize the shock train dynamics. In this section, Mach disk height variation due to the perturbation for different chamber pressure, laser energy, and deposition locations, as listed in Table 1, are discussed in detail.

3.1.1. Energy Deposition at the Nozzle Exit

As described in Section 2, the energy deposition at the nozzle exit is used to examine the effect of energy deposition on the shock reflection and Mach disk height variation. Figure 3 shows a typical sequence of the shock train dynamics after the energy deposition (578 mJ) at the nozzle exit and chamber pressure of $P_C = 689$ kPa. The perturbation to the shock train is the combined effect of the shock wave generated by the energy deposition and the interaction of the jet fluid with the hot plasma. Due to the energy deposition, the temperature in the location increases and changes the local Mach number, which also acts as a perturbation to the flow. The perturbation, both in terms of the laser-induced shock wave and the local hot spot, is very short-lived, on the order of 125 µs, as the shock wave propagates away and the hot spot is convected downstream at the flow velocity. The laser energy deposition, cone angle variation, Mach disk height and width variation, the hot zone transportation by the jet flow, and the recovery and stabilization of the shock train are evident in the sequence.

The energy deposition is visible at $t = 31.25$ µs as a bright spot at the exit of the nozzle. The Mach disk height is obtained by measuring the distance from the first shock interaction about the nozzle exit plane. The variation of the Mach disk height is used to characterize the dynamics of the shock train. It is observed that the energy deposition disrupts the jet and the shock train during the perturbation at $t = 62.5$ µs, and the flow regains its initial characteristics, i.e. the Mach reflection, shortly after that. By closely observing the variation in the Mach disk width in the sequence, it is

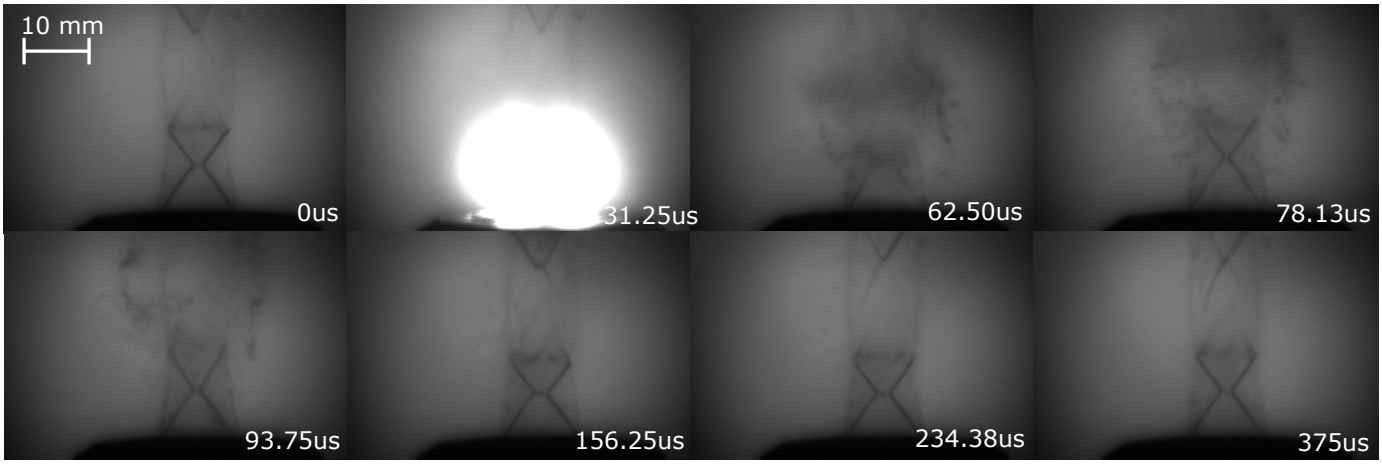

Figure 3. Shock train dynamics due to the energy deposition (578 mJ) at nozzle exit, and $P_C = 689$ kPa.

evident that the shock structure momentarily changes from its initial character to regular reflection at $t = 78.13$ µs, and then returns to its initial state by $t = 156.25$ µs. This transition from Mach to regular reflection is due to the interaction between the shock wave and hot plasma zone generated within the jet as well as the sudden rise in pressure at the exit of the nozzle due to the energy deposition. However, the incoming flow pushes the perturbation and the hot plasma away from the deposition location, leading to the recovery of the steady flow state. This transition from Mach to regular reflection and later the recovery of the flow causes the stretching and relaxation of the shocks and variation of the Mach disk height which is also noticeable in Fig. 4 as the high peaks near the deposition location.

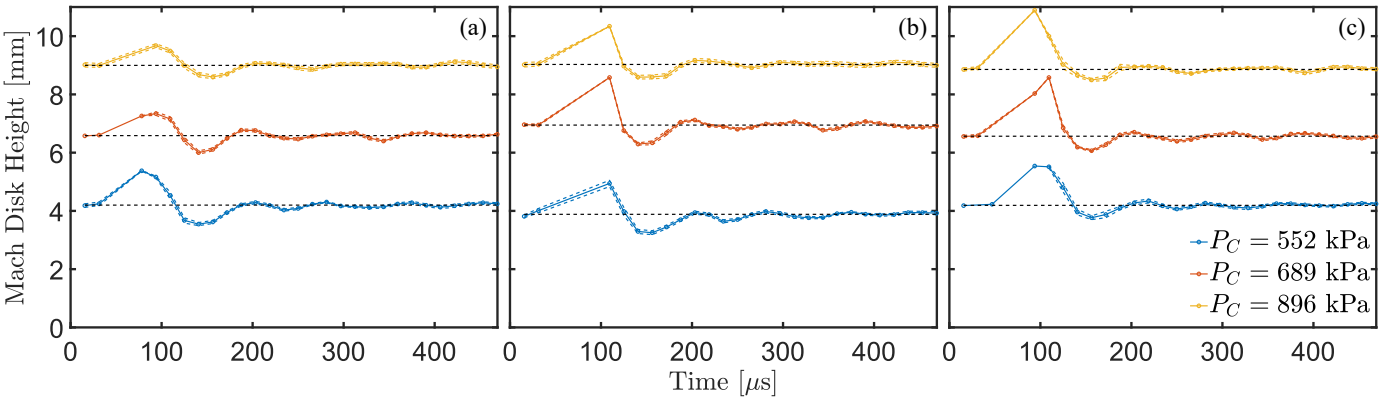

Figure 4. Instantaneous Mach disk height variation due to laser energy, (a) 272 mJ, (b) 578 mJ, and (c) 716 mJ, at location 1

Figure 4 shows the variation of the Mach disk height due to the laser energy deposition at the nozzle exit for different laser pulse energies. Intuitively, the Mach disk height shows an increasing trend with the chamber pressure where it is the lowest at $P_C = 552$ kPa and highest at $P_C = 896$ kPa. Moreover, damped oscillations appear in the Mach disk height variation, and similar behavior is also seen for other chamber pressure conditions. It is also evident from the figure that

the maximum amplitude of the oscillations increases with the energy of the laser. However, the frequency of the damped oscillations is found to be the same for all cases, approximately 10 kHz. It implies that the frequency of the oscillations in a supersonic jet due to the perturbation remains constant, and independent of the strength of the perturbation and chamber pressure. The highest amplitude of the oscillations is observed immediately after the energy deposition. The incoming flow pushes the perturbation and the hot plasma away from the deposition location, leading to the recovery of the steady flow state. The time from the initial peak to the flow steady state for chamber pressure $P_C = 552$ kPa, 689 kPa, and 896 kPa are found around 400 µs, 400 µs, and 300 µs respectively. The recovery of an over-expanding supersonic jet to its steady state due to the perturbation at the nozzle exit is a function of the chamber pressure independent of the disturbance energy, and the process of recovery is accelerated with an increase in the chamber pressure.

3.1.2. Energy Deposition at the Pre-reflection Point

The effect of the perturbation on the shock structure is investigated by depositing the laser energy just below the reflection point, i.e. the pre-reflection point. Figure 5 shows the variation in the Mach disk height due to the energy deposition at location 2. It is evident from the figure that the Mach disk height follows a similar trend as in the nozzle exit case including the time for flow recovery for different chamber pressures. However, the magnitudes of the highest peak in the Mach disk height variation of pre-reflection cases are relatively lower than the corresponding case with the disturbance at the nozzle exit. The frequency of the oscillations is again found to be the same for all cases and independent of the chamber pressure and laser energy, approximately 10 kHz.

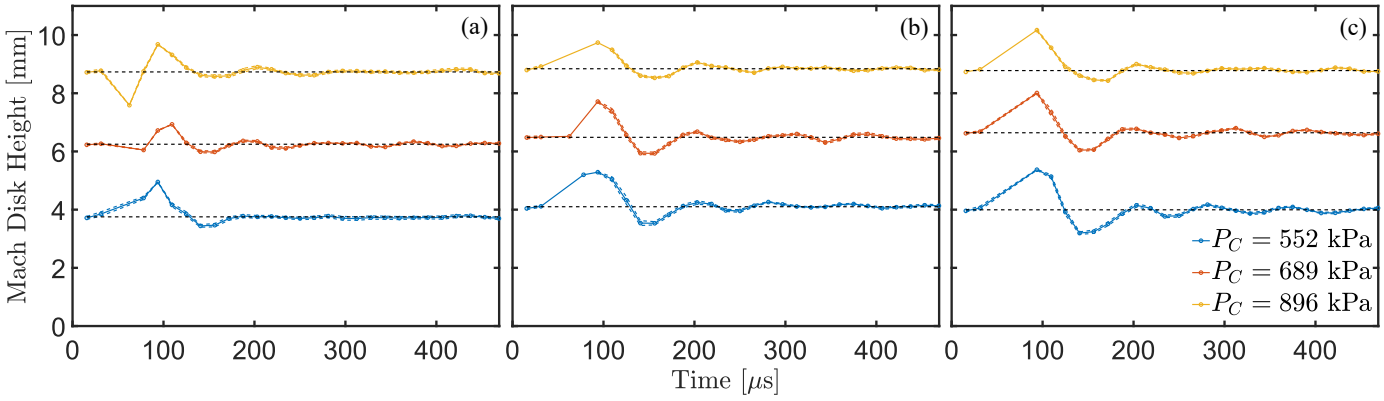

Figure 5. Instantaneous Mach disk height variation for the laser energy, (a) 272 mJ, (b) 578 mJ, and (c) 716 mJ, at the pre-reflection point

A typical sequence of the shock structure dynamics due to the laser energy deposition at location 2 for $P_C = 689$ kPa and 578 mJ laser energy is shown in Fig. 6. The energy deposition, $t = 15.63$ µs, transition of the shock reflection, $t = 78.13$ µs, and the flow structure recovery, $t = 156.25$ µs, can

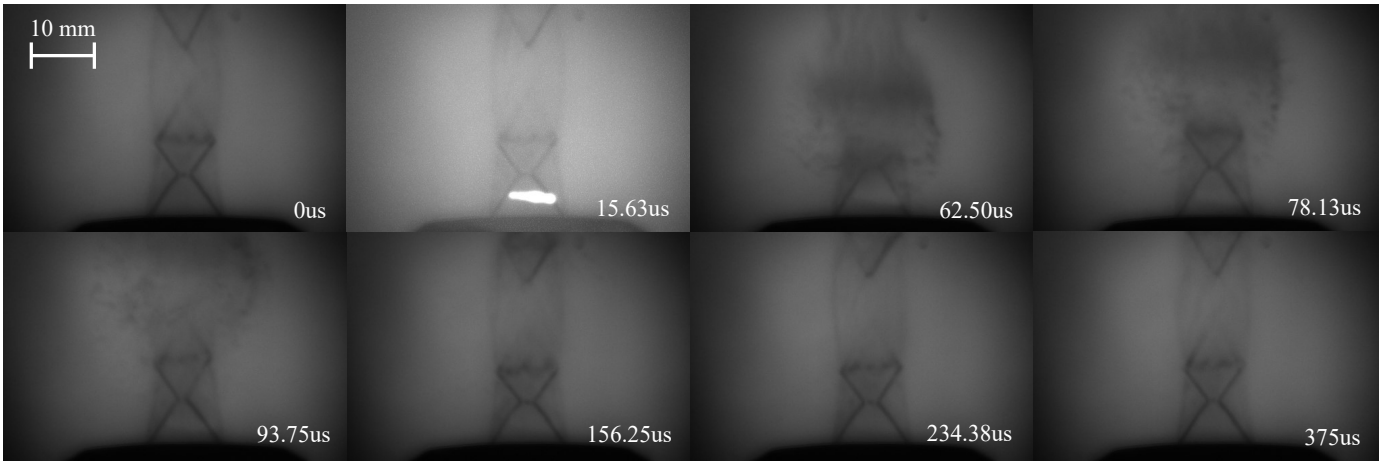

Figure 6. Shock train dynamics due to the energy deposition (578 mJ) at the pre-reflection point, and $P_C = 689$ kPa

identified from the image sequence. A detailed analysis of the transition of the shock reflection due to perturbation at the pre-reflection point is provided in Sec. 3.2. From the image sequences of nozzle exit and pre-reflection point scenarios, no significant difference in the shock dynamics is evident except for the location of the energy deposition.

3.1.3. Energy Deposition at the Post-reflection Point

Figure 6 shows the Mach disk height variation induced by the perturbation of flow structure at the post-reflection point for different laser energy levels and chamber pressure. Unlike the previous two cases, in this case, a sudden drop in the Mach disk height is observed before the highest peak for all laser energy levels. This drop in the Mach disk height results from the interaction between the laser-induced shock wave and the first reflection as the shock from the energy deposition pushes gas downwards towards the nozzle. The Mach disk height followed a similar trend as in the other two cases where the amplitude of the Mach disk height linearly varies with the laser energy for all chamber pressures. As in the pre-reflection case, a noticeable reduction in the maximum amplitudes of the highest peak is visible in the Mach disk height variations, indicating a weaker effect on the shock structure compared to the other energy deposition locations. For all laser energy levels, the time taken to regain the flow steady state from the disruption for the chamber pressure of $P_C = 552$ kPa, 689 kPa, and 896 kPa is around 400 µs, 300 µs, and 250 µs, respectively. Compared to the energy deposition at the nozzle exit and pre-reflection point, oscillations induced by the perturbation are dampened relatively quickly at the post-reflection point cases, implying an elevated response of the jet to the perturbation. The frequency of the oscillations is once again found to be 10 kHz for all cases irrespective of the chamber pressure and laser energy.

The laser energy deposition, cone angle variation, Mach disk height and width variation, the hot

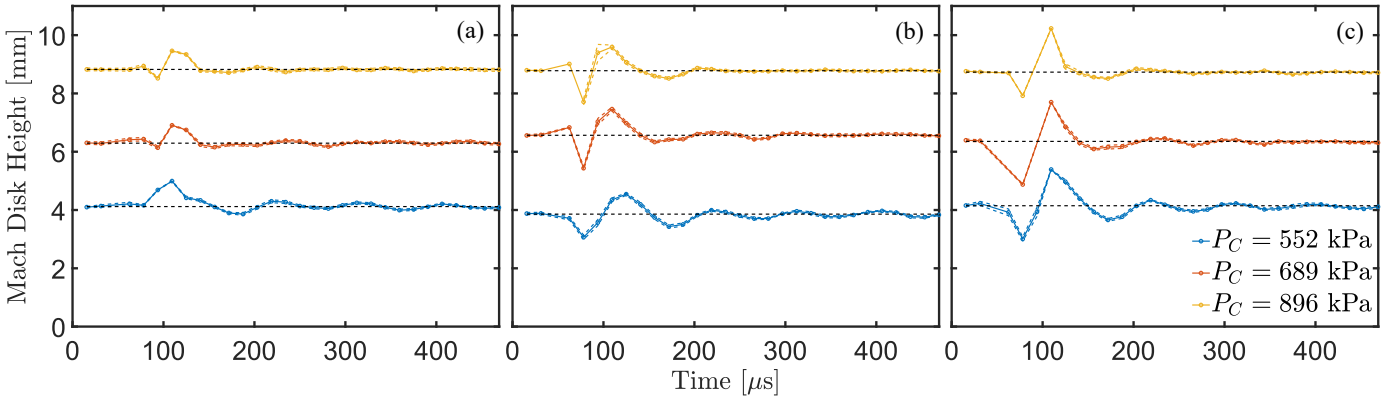

Figure 7. Instantaneous Mach disk height variation for the laser energy, (a) 272 mJ, (b) 578 mJ, and (c) 716 mJ, at post-reflection point

zone transportation, and the recovery of the shock train for the post-reflection laser energy deposition are seen in Fig. 8. The sudden drop in the Mach disk height due to the interaction between the Mach reflection and shock wave produced by the laser spark is apparent at $t = 62.5$ µs. The recovery of the shock structure along with the transition of the Mach to regular reflection is also noticeable in the image sequence. Further analysis of the transition is provided in Sec. 3.2.

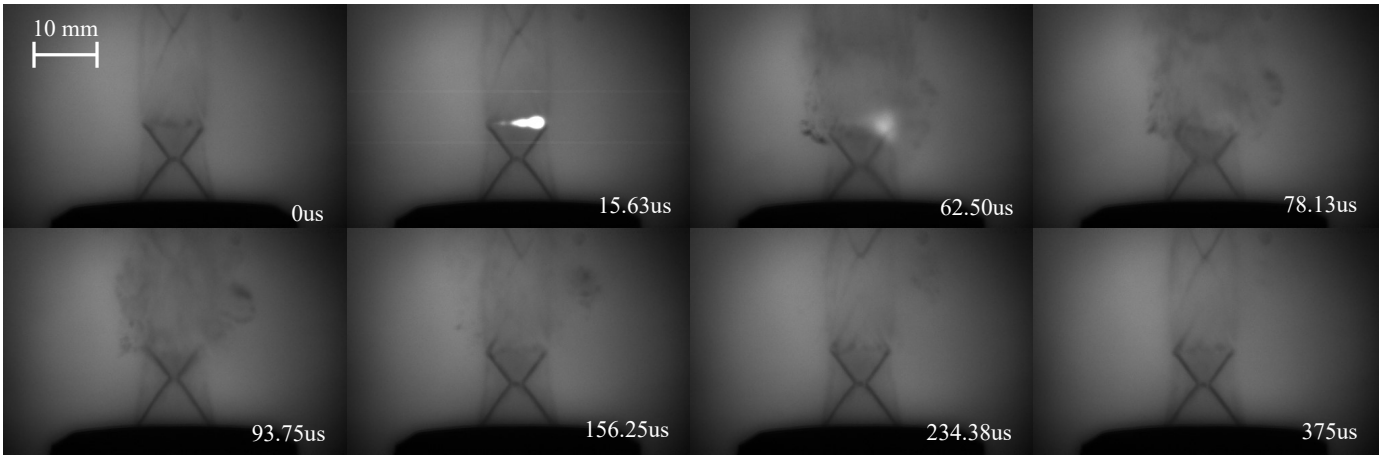

Figure 8. Shock train dynamics due to the energy deposition (578 mJ) at the post-reflection point, and $P_C = 689$ kPa

3.1.4. Oscillation Analysis

A damping ratio is introduced to characterize the response of the supersonic jet to the perturbation induced by the laser energy deposition. The damping ratio is modeled after a damped oscillator, and is defined as the ratio of actual damping of oscillation to critical damping. In critical damping, the system will reach its steady state without exhibiting any oscillatory behavior whereas in an under-damped case, the system attains its steady state after several oscillations with decaying magnitude.

$$\text{Damping Ratio} = \frac{\text{Actual Damping}}{\text{Critical Damping}}$$

$$\text{Damping Ratio } (\zeta) = \frac{1}{\sqrt{1 + (\frac{2\pi}{\delta})^2}}$$

Where δ is the logarithmic decrement, defined as $\delta = \log\left(\frac{x_2}{x_1}\right)$, where x_2 and x_1 are two successive peaks of the oscillation. The damping ratio is always less than 1 for an under-damped case.

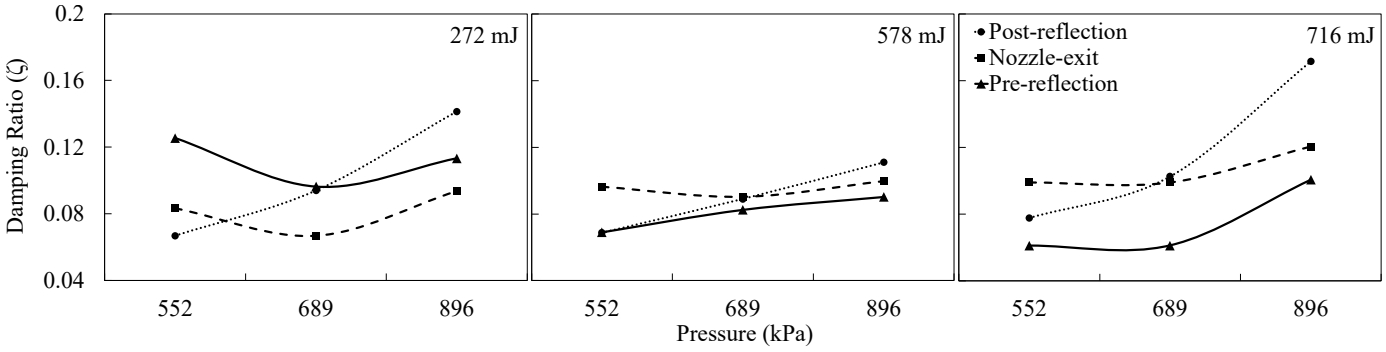

Figure 9. Damping ratio of the oscillations at different laser energies 272 mJ (left), 578 mJ (center), and 716 mJ (right)

Figure 9 shows the damping ratio of the oscillations obtained for the nozzle exit, pre-reflection, and post-reflection cases for different chamber pressures and laser energy levels. A nearly linear variation of the damping ratio with chamber pressure is observed for all laser energy levels and deposition locations. For the post-reflection point, the perturbation induced by the 272 mJ laser energy shows a linear increase in damping ratio from 0.06 to 0.14 with respect to the chamber pressure which implies that the oscillations decay faster at higher chamber pressures, consistent with the observations in the previous sections. In the nozzle exit and pre-reflection point cases, the damping ratio remains nearly constant at all pressures with an average of 0.08 for nozzle exit and 0.11 for pre-reflection point cases. A similar trend is observed in the damping ratios of the nozzle exit, pre-reflection, and post-reflection at 578 mJ and 716 mJ pulse energies. Moreover, the relative difference in the damping ratio among the deposition locations reaches a minimum at 578 mJ laser energy case, and the difference is larger for the other laser energy levels.

3.2. Shock Reflection and Transition

Reflection transition, i.e. Mach-to-regular and regular-to-Mach reflections, is observed in a number of experimental conditions. They were associated with the recovery of the jet steady state from the oscillatory behavior which is induced by the energy deposition. The perturbation results in an abrupt change to the characteristics of the jet flow and shock structure and leads to the transition of the shock reflection depending on the flow condition. It is observed that at steady state and during

the flow recovery, both $P_C = 552$ kPa and $P_C = 896$ kPa cases exhibit only Mach reflection or regular reflection respectively. At the low chamber pressure conditions, the perturbation induced by the laser energy deposition is not sufficient to support the transition of the shock reflection. When the chamber pressure is high enough, however, the jet flow is strong enough to overcome the disturbance resulting from the energy deposition without altering the characteristics of the shock structure. However, the transition of Mach to regular reflection or vice versa is witnessed for the medium chamber pressure condition, i.e. at $P_C = 689$ kPa, for all laser energy levels. Figure 10 shows typical shock reflections and transitions observed at the nozzle exit, pre-reflection, and post-reflection points in medium chamber pressure condition, i.e. $P_C = 689$ kPa, and 578 mJ laser energy.

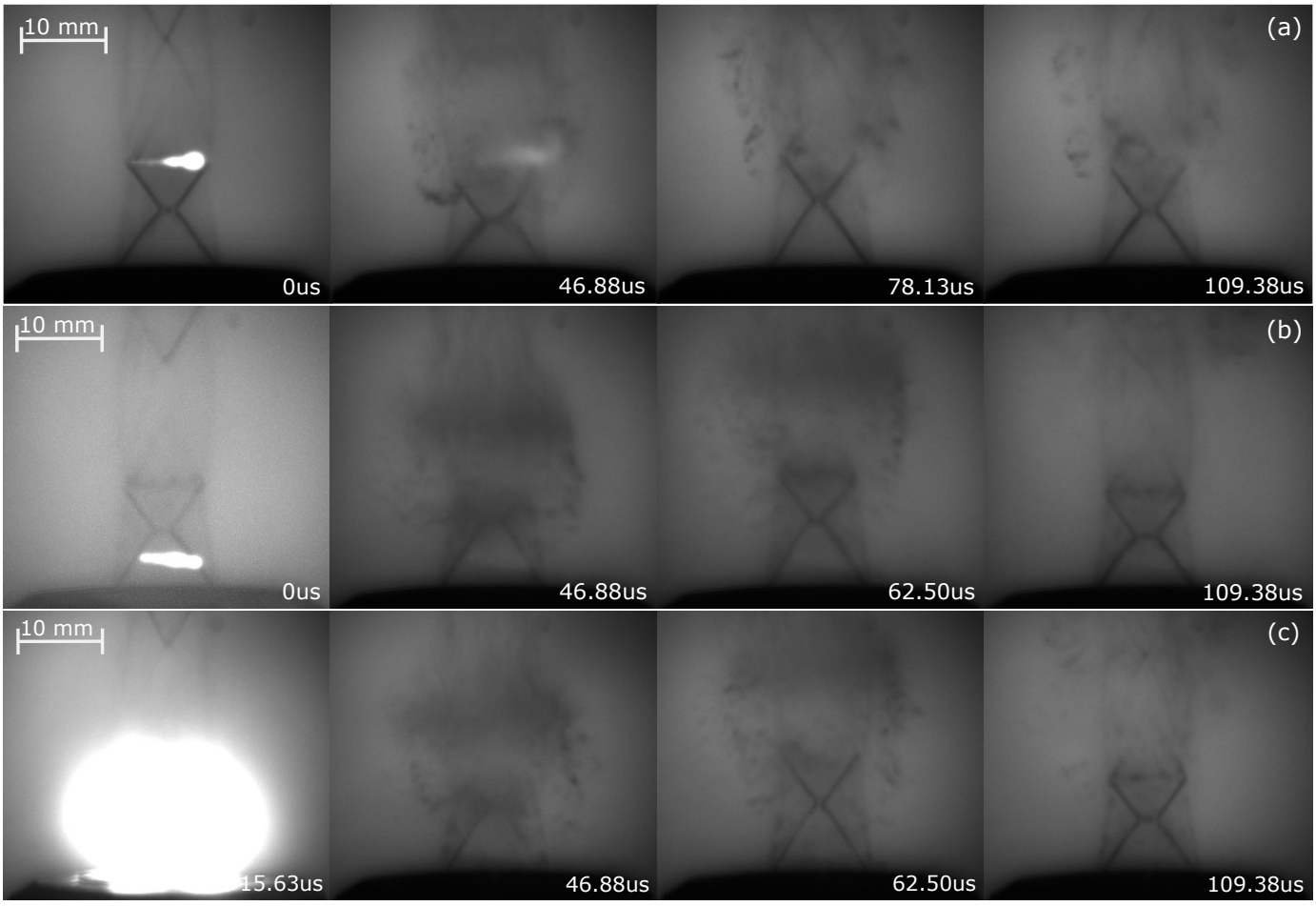

Figure 10. Transition of the shock reflection due to energy deposition (578 mJ) at (a) post-reflection, (b) pre-reflection, and (c) nozzle exit, and at $P_C = 689$ kPa

A noticeable similarity in the shock transition is observed for the nozzle exit and pre-reflection cases, Fig. 10 (b) and (c). In both cases, the recovering jet flow sweeps away the hot zone generated by the energy deposition at 46.88 µs after the deposition. The Mach reflection behavior visible in this instance may be due to an instantaneous rise in back pressure due to the shock wave generated

by the laser spark and the associated local temperature and density deviation. This argument is further strengthened by the transition of the shock structure from Mach reflection to regular reflection at 62.5 µs. The shock train regains its initial structure at 109.8 µs through the transition from regular to Mach reflection.

A distinct feature of the shock structure with the spark at the post-reflection point is the transformation of regular reflection at this chamber pressure to a strong Mach reflection at 46.88 µs, Fig. 10 (a). This transformation in the shock structure is attributed to the interaction between the Mach reflection and the shock wave generated by the laser-induced breakdown. The expanding shock wave creates a high-pressure zone behind the Mach reflection instantaneously and forces the transformation witnessed in the sequence. There is then a transition from Mach to regular reflection at 78.13 µs. The recovery of the initial shock structure is seen at 109.38 µs.

4. Conclusion

In this study, experimental investigations are performed to understand the influence of perturbations due to short-duration energy deposition on the shock train structure of an axisymmetric over-expanded jet. The flow is perturbed by the laser-induced breakdown, creating a shock wave and a high-temperature plasma zone in the shock train. A high-speed self-aligning focusing schlieren system is used to visualize the flow structure variations by measuring the Mach disk height to characterize the shock train dynamics and the flow structure recovery process.

Both Mach disk height and image sequence analysis indicate the response of jet flow to the energy deposition at the nozzle exit and the pre-reflection point is similar for the deposition of energy anywhere inside the first shock reflection. The magnitude of the highest peak in the Mach disk height variation is reduced with deposition location further downstream. A significant difference in the response of the over-expanded jet is observed in the post-reflection energy deposition where the Mach disk shows a sudden drop in height immediately after the deposition. This drop is due to the interaction between the laser-induced shock wave and the first shock reflection at the post-reflection point. The frequency of the oscillations of the Mach disk height is found to be the same for all cases and irrespective of the chamber pressure, laser energy, and deposition location, approximately 10 kHz.

The damping ratio is used to characterize the oscillatory behavior observed in the Mach disk height variation due to the perturbation. For the pre-reflection point and nozzle exit cases, it is found to be nearly constant for all scenarios whereas, it increases nearly linearly with the chamber pressure for the post-reflection cases. The transition of Mach to regular reflection and vice versa are observed at a chamber pressure of $P_C = 689$ kPa because this pressure is close to the bifurcation point between Mach and regular reflection at steady state.

References

Anderson, J. D. (1990). *Modern Compressible Flow: With Historical Perspective* (Vol. 12). McGraw-Hill New York.

Bathel, B. F., & Weisberger, J. M. (2022). Development of a self-aligned compact focusing schlieren system for nasa test facilities. In *AIAA SciTech 2022 Forum* (p. 0560).

Ben-Dor, G. (2013). Hysteresis phenomena in reflection of shock waves. In *International Symposium on Shock Waves* (pp. 3–10).

Ben-Dor, G., Ivanov, M., Vasilev, E., & Elperin, T. (2002). Hysteresis processes in the regular reflection↔mach reflection transition in steady flows. *Progress in Aerospace Sciences*, *38*(4-5), 347–387.

Hadjadj, A., Kudryavtsev, A., & Ivanov, M. (2004). Numerical investigation of shock-reflection phenomena in overexpanded supersonic jets. *AIAA journal*, *42*(3), 570–577.

Hornung, H. (1986). Regular and mach reflection of shock waves. *Annual Review of Fluid Mechanics*, *18*(1), 33–58.

Ivanov, M., Khotyanovsky, D., Kudryavtsev, A., Nikiforov, S., & Trotsyuk, A. V. (2004). Hysteresis-related phenomena in shock wave reflection. In *Proceedings of the 21st international Congress of Theoretical and Applied Mechanics.*

Joarder, R. (2019). On the mechanism of wave drag reduction by concentrated laser energy deposition in supersonic flows over a blunt body. *Shock Waves*, *29*(4), 487–497.

Joarder, R., Padhi, U. P., Singh, A. P., & Tummalapalli, H. (2017). Two-dimensional numerical simulations on laser energy depositions in a supersonic flow over a semi-circular body. *International Journal of Heat and Mass Transfer*, *105*, 723–740.

Knight, D., Elliott, G., Candler, G., & Zheltovodov, A. (2003). Localized flow control in high speed flows using laser energy deposition. *CCD*, *25*, 2003.

Matsuo, S., Setoguchi, T., Nagao, J., Alam, M. M. A., & Kim, H. D. (2011). Experimental study on hysteresis phenomena of shock wave structure in an over-expanded axisymmetric jet. *Journal of Mechanical Science and Technology*, *25*, 2559–2565.

Mouton, C. A., & Hornung, H. G. (2008). Experiments on the mechanism of inducing transition between regular and mach reflection. *Physics of Fluids*, *20*(12).

Paramanantham, V., Janakiram, S., & Gopalapillai, R. (2022). Prediction of mach stem height in compressible open jets. part 1. overexpanded jets. *Journal of Fluid Mechanics*, *942*, A48.

Phuoc, T. X. (2006). Laser-induced spark ignition fundamental and applications. *Optics and Lasers in Engineering*, *44*(5), 351–397.

Phuoc, T. X., & White, F. P. (2002). An optical and spectroscopic study of laser-induced sparks to determine available ignition energy. *Proceedings of the Combustion Institute*, *29*(2), 1621–1628.

Shimshi, E., Ben-Dor, G., & Levy, A. (2009). Viscous simulation of shock-reflection hysteresis in overexpanded planar nozzles. *Journal of Fluid Mechanics*, *635*, 189–206.

Singh, A. P., Padhi, U. P., Tummalapalli, H., & Joarder, R. (2017). Investigations on ignition of atomized fuel-air mixtures and liquid fuel column-air combinations by low energy laser pulses. In *Asia-Pacific Conf. Combust., The Combustion Institute, Sydney.*

Takayama, K., & Ben-Dor, G. (1993). State-of-the-art in research on mach reflection of shock waves. *Sadhana*, *18*, 695–710.

Wang, D., & Yu, Y. (2015). Shock wave configurations and reflection hysteresis outside a planar laval nozzle. *Chinese Journal of Aeronautics*, *28*(5), 1362–1371.

Yan, H., Adelgren, R., Elliott, G., Knight, D., & Beutner, T. (2003). Effect of energy addition on mr rr transition. *Shock Waves*, *13*(2), 113–121.

Yan, H., Adelgren, R., Elliott, G., Knight, D., Buetne, T., & Ivanov, M. (2002). Laser energy deposition in intersecting shocks. In *1st Flow Control Conference* (p. 2729).

Yang, L. (2012). *Flow Control using Energy Deposition at Mach 5*. The University of Manchester (United Kingdom).

Zmijanović, V., Rašuo, B., & Chpoun, A. (2012). Flow separation modes and side phenomena in an overexpanded nozzle. *FME Transactions*, *40*(3), 111–118.